Particle and Fibre Toxicology

RESEARCH

Open Access

Polystyrene nanoplastics exposure induces cognitive impairment in mice via induction of oxidative stress and ERK/MAPK-mediated neuronal cuproptosis

Yinuo Chen[1†], Yiyang Nan[1†], Lang Xu[1,2†], Anqi Dai[1], Rosa Maria Martinez Orteg[3], Mantong Ma[4], Yan Zeng[1*] and Jinquan Li[1,2*]

Abstract

Background Recent studies emphasize the significance of copper dyshomeostasis in neurodegenerative diseases, such as Alzheimer's and Parkinson's, thereby highlighting the role of copper in neurotoxicity. Cuproptosis, a novel mechanism of copper-dependent cell death, remains underexplored, particularly concerning environmental pollutants like polystyrene nanoplastics (PS-NPs). While PS-NPs are recognized for inducing neurotoxicity through various forms of cell death, including apoptosis and ferroptosis, their potential to trigger neuronal cuproptosis has not yet been investigated. This study aims to determine whether exposure to PS-NPs induces neurotoxicity via cuproptosis and to explore the preliminary molecular mechanisms involved, thereby addressing this significant knowledge gap.

Methods Seven-week-old male C57BL/6 mice were exposed to PS-NPs at dose of 12.5 mg/kg, and were co-treated with the antioxidant N-acetylcysteine (NAC). Complementary in vitro experiments were conducted using SH-SY5Y neuronal cells exposed to PS-NPs at a concentration of 0.75 mg/mL, with interventions that included the copper chelator tetrathiomolybdate (TTM), NAC, and the MAPK inhibitor PD98059.

Results Exposure to PS-NPs significantly increased cerebral copper accumulation ($P < 0.05$) and induced cuproptosis, characterized by lipid-acylated DLAT oligomerization, dysregulation of cuproptosis regulators (FDX1, LIAS, HSP70), and mitochondrial damage. In murine models, PS-NPs elicited neurotoxicity, as evidenced by neuronal loss, decreased Nissl body density, impaired synaptic plasticity, and suppressed oxidative stress markers (GSH, SOD, Nrf2), alongside activation of the ERK-MAPK pathway, ultimately resulting in deficits in learning and memory. Treatment with NAC alleviated these adverse effects. In SH-SY5Y cells, exposure to PS-NPs resulted in reduced cell viability ($p < 0.01$), an

†Yinuo Chen, Yiyang Nan and Lang Xu contributed equally to this work.

*Correspondence:
Yan Zeng
zengyan68@wust.edu.cn
Jinquan Li
Lijinquan@wust.edu.cn

Full list of author information is available at the end of the article

effect that was mitigated by TTM. Furthermore, NAC and PD98059 were found to reverse elevated copper levels, cuproptosis markers, and mitochondrial anomalies ($p < 0.05$).

Conclusion This study presents preliminary evidence indicating that PS-NPs may induce neuronal cuproptosis, potentially through the oxidative stress-mediated activation of the ERK-MAPK pathway, which contributes to cognitive dysfunction in mice. These findings provide insights into the potential mechanisms underlying PS-NPs neurotoxicity and highlight possible therapeutic targets, such as copper chelation or MAPK inhibition, for mitigating the neurological risks associated with nanoplastic exposure, pending further validation in human-relevant models.

Graphical abstract

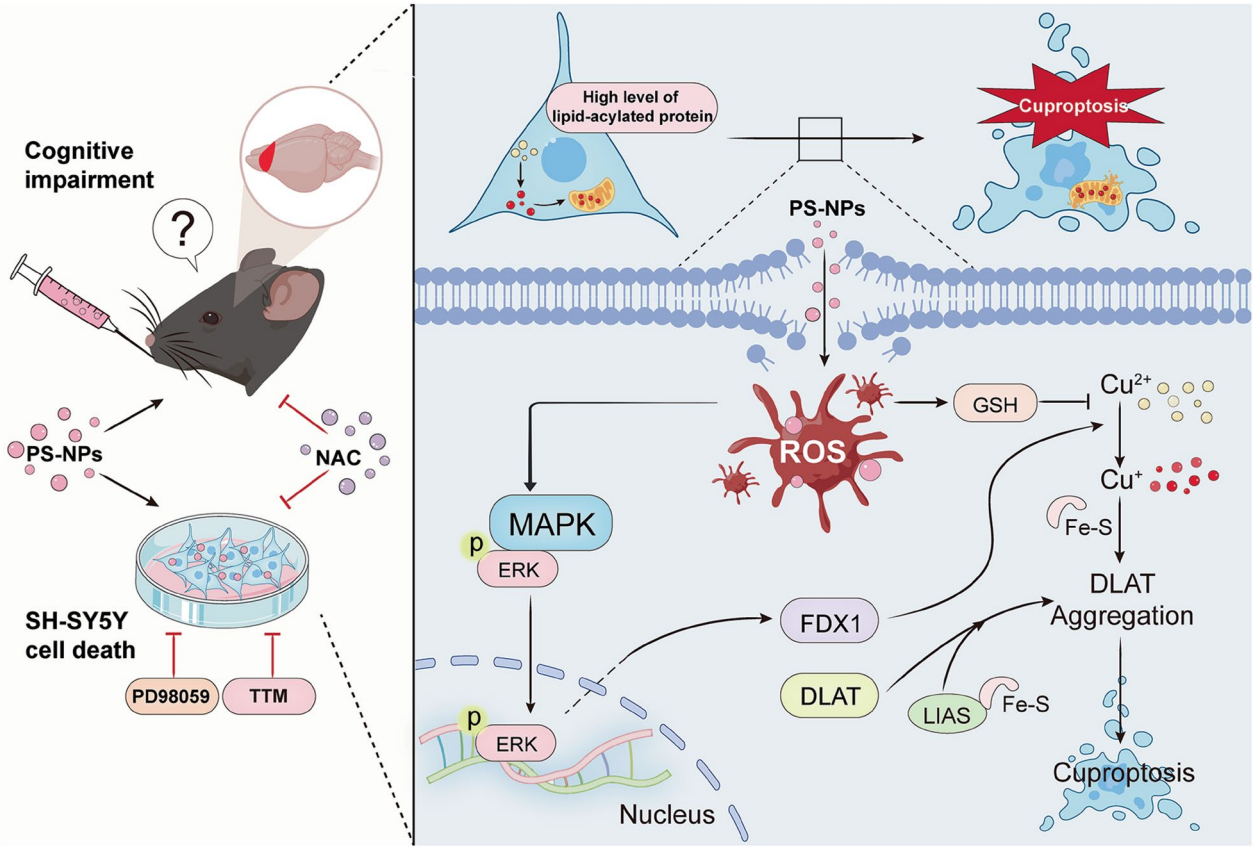

Keywords Polystyrene nanoplastics, Cuproptosis, Oxidative stress, Cognitive dysfunction, ERK-MAPK

Background

Issues arising from microplastic particle (MP) pollution are a significant and global public health concern, polystyrene is among the most widely used plastics. Humans may ingest average quantities of 0.1–5 g of MPs weekly [1]. These particles can infiltrate vital organs, including the heart, liver, and kidneys, via the bloodstream [2], and even breach the blood–brain barrier and enter the central nervous system within 2 h of ingestion [3]. Oral exposure is the primary route through which microplastics enter the human body [4]. Multiple animal studies have demonstrated that oral exposure to nanoplastics increases the permeability of the blood-brain barrier, facilitates their distribution in the brain, drives neurotoxicity and neurodegeneration, and ultimately impairs brain function [5, 6]. Links between exposure to MPs and the onset of neurodegenerative disorders are well established [7], which can include conditions such as Parkinson's [8] and Alzheimer's diseases [9]. Since smaller nanoplastic particles (NPs) have a large specific surface area, they can easily penetrate cell membranes and be taken up by cells, and then accumulate in various tissues and organs, causing greater toxicity [10, 11]. Therefore, understanding the neurotoxicity of NPs, and their underlying mechanisms is needed for effective prevention and control.

Excessive activation of regulated cell death pathways such as apoptosis, ferroptosis, and pyroptosis contributes directly to development of diseases associated with cognitive dysfunction [12, 13]. Exposure to PS-NPs can induce tissue damage by triggering apoptosis, ferroptosis, and pyroptosis, and affect organ function [14–16]. Cuproptosis, a form of programmed cell death that involves the interference of copper ions with the lipoylation process in the tricarboxylic acid (TCA) cycle, also contributes to neurological disorders [17, 18]. Although copper is an essential cofactor for all living organisms, it becomes toxic at concentrations that exceed levels regulated by evolutionarily conserved homeostatic mechanisms [19]. Serum levels of copper ions are elevated in patients with Parkinson's disease compared with healthy individuals [20], and abnormalities in copper ion levels also occur in the cerebrospinal fluid of early stage Huntington's disease patients [21]. Additionally, formation of amyloid-beta (Aβ) plaques in the brain of Alzheimer's disease models is significantly associated with alterations in copper levels [22]. When excessive copper ion accumulates within cells it binds to lipases in the TCA cycle, triggering thiooctanoylated protein aggregation and the loss of iron-sulfur (Fe-S) cluster proteins, leading to proteotoxic stress and cell death. Excessive copper accumulation may trigger oxidative stress [23], which may activate the mitogen-activated protein kinase (MAPK) cascade, a common regulator of cell death and stress responses, including extracellular signal-regulated kinase (ERK), c-jun N-terminal kinase (JNK), and p38, and is associated with cuproptosis-related genes in Alzheimer's disease [24, 25]. Polystyrene nanoplastics, ubiquitous environmental pollutants, are well-documented to induce oxidative damage in the central nervous system and trigger various forms of cell death, such as apoptosis and ferroptosis [26], resulting in neurotoxicity-a recognized contributor to neurodegenerative diseases. However, whether PS-NPs induce neurotoxicity through neuronal cuproptosis, a novel copper-dependent cell death pathway, and the underlying molecular mechanisms remain to be systematically investigated.

In this study, we established a 30-day exposure model of PS-NPs in mice. We employed behavioral tests, including the water maze, along with pathological assessments such as hematoxylin and eosin (H&E) staining, to elucidate cognitive function and damage in the prefrontal cortex of the model mice. Subsequently, we measured copper levels and key markers of cuproptosis, including Ferredoxin 1 (FDX1), to assess the extent of neuronal cuproptosis following PS-NPs exposure. Furthermore, we conducted KEGG pathway enrichment analysis using transcriptome data from the prefrontal cortex of PS-NPs-exposed mice to identify the role of the MAPK pathway in interaction with PS-NPs. Finally, we utilized the copper ion chelator tetrathiomolybdate (TTM), the antioxidant N-acetylcysteine (NAC), and ERK inhibitors to clarify our hypothesis that PS-NPs could activate the MAPK pathway by inducing oxidative stress, which triggers neuronal cuproptosis and ultimately leads to cognitive impairment.

Methods

Characterizations of PS-NPs

Polystyrene nanoplastics (2.5% w/v, 10 ml, 60 nm) were purchased from Tianjin BaseLine Chrom Tech Research Center (Tianjin, China). Before use, PS-NPs were dispersed in distilled water, and their shape, size, and zeta potential were verified by scanning microscope (IT700HR, Japan) and zeta potentiostat (Zetasizer Nano S90, Malvern, UK).

Animals and treatments

Male C57BL/6 mice (7 weeks, 20–22 g), purchased from the Hubei Provincial Laboratory Animal Center, housed at the Wuhan University of Science and Technology (WUST) Animal Center (Wuhan, China), were maintained in standard environments with a 12:12 h light/ dark cycle at 22 °C, and ate and drank ad libitum until experimentation. Experimental protocols followed guidelines on the care and use of laboratory animals, with experimentation approved by the WUST Ethics Committee. Mice were divided into four treatments of 27 individuals: (1) control; (2) 12.5 mg/kg/d PS-NPs; (3) 2 g/L NAC; and (4) 12.5 mg/kg/d PS-NPs + 2 g/L NAC. Mice in treatments 2, and 4 were gavaged with 60 nm PS-NPs by body weight daily for 30 d; mice in treatment 1 were given equal volumes of distilled water in the same way; mice in treatments 3 and 4 were given 2 g/L NAC aqueous solution from day 1 for 30 d. (Globally, the estimated weekly intake of microplastics ranges from 0.1 to 5 g per person, with a corresponding daily intake of 0.23–11.9 mg/kg body weight, assuming an average human body weight of 60 kg [1]. To translate the human exposure dose to an equivalent dose in mice, we employed a body surface area-based conversion formula: mouse equivalent dose (mg/kg) = human dose (mg/kg) × [Km (human)/Km (mouse)], where the Km factor is defined as body weight (kg) divided by body surface area (m^2) [27]. Based on established data, the body surface areas for humans and mice are 1.62 m^2 and 0.007 m^2, respectively, with corresponding body weights of 60 kg and 0.02 kg [28, 29]. Thus, for a 0.02 kg mouse, the calculated equivalent dose ranges from 0.05 to 2.9 mg/day. In our study, we administered a dose of 12.5 mg/kg/day, which corresponds to a daily microplastic intake of 0.25 mg per mouse).

To systematically assess the effects of PS-NPs exposure, this study implemented a structured experimental protocol. Mice were subjected to a 30-day exposure

period with daily fixed-time administration of PS-NPs and NAC. Seven mice ($N=7$) were randomly selected to undergo sequential behavioral assessments as follows: Novel Object Recognition testing from days 31 to 33; Y-maze testing on day 34; Morris Water Maze training from days 35 to 39; and the MWM probe test on day 41. On day 31, the remaining 20 mice ($N=20$) were euthanized for subsequent tissue collection experiments. Due to variations in tissue processing methods and homogenate requirements for different assays, mice from each treatment group were assigned using a completely randomized grouping method following exposure, with procedures detailed as follows: (1) Three mice ($N=3$) were anesthetized and cardiac perfused with saline, the brains were removed and fixed in 4% paraformaldehyde, embedded in paraffin and prepared for sectioning, and 3 consecutive 5-μm-thick cryosections were prepared from the PFC of each animal to cover an anatomical range of + 1.77 to + 1.33 mm in the Bregma, and used for immunohistochemistry (NRF2), immunofluorescence (DLAT), H&E staining and Nissl staining. (2) Three mice ($N=3$) were euthanized, and their brains were immediately extracted, with the PFC isolated for total RNA extraction per kit instructions, followed by mRNA expression analysis. (3) Three mice ($N=3$) were euthanized, and their PFCs were isolated, lysed, homogenized, and quantified using the BCA method for subsequent Western Blot analysis. (4) Three mice ($N=3$) were anesthetized and sequentially perfused with saline and electron microscopy fixative; their PFCs were isolated, trimmed into small blocks, fixed, and processed into ultrathin sections for staining and transmission electron microscopy observation. (5) Three mice ($N=3$) were euthanized, and their PFCs were isolated for RNA sequencing. (6) Five mice ($N=5$) were euthanized, and their brains were homogenized for quantification of glutathione (GSH), superoxide dismutase (SOD) activity, and copper ion levels using respective assay kits. All mice were euthanized with pentobarbital sodium, and brain tissues were harvested. This experimental design and sampling strategy ensured systematic behavioral evaluation, randomized tissue allocation, and representative analyses.

Cell culture and treatment

Human neuroblastoma cell line (SH-SY5Y) was purchased from the Chinese Academy of Medical Sciences (CAMS) and cultured in Dulbecco's modified Eagle's medium (Gibco, MA, USA) supplemented with 10% fetal bovine serum (Gibco, MA) at 37 °C with 5% carbon dioxide; After 24 h of plating, differentiation was initiated by reducing FBS in the culture medium to 1% and supplementing with 10 μM Retinoic acid (RA) for 7 days [30]. Relevant experimental operations were performed in a standard cell culture room.

RA, NAC, ERK inhibitor PD98059, and copper ion chelator (ammonium tetrathiomolybdate (TTM)) were purchased from MedChemExpress (Shanghai, China). SH-SY5Y cells were cultured with PS-NPs (0.75 mg/mL); NAC (5 μM); PS-NPs (0.75 mg/mL) + NAC (5 μM); PD98059 (5 μM); PS-NPs (0.75 mg/mL) + PD98059 (5 μM); TTM (2 μM); and PS-NPs (0.75 mg/mL) + TTM (2 μM) for 24 h.

Cell viability assay

Well-grown SH-SY5Y cells were inoculated into 96-well cell culture plates at cell densities of 5×10^3/well. After 24 h, SY5Y cells were treated with different concentrations of PS-NPs (0,0.25, 0.5, 0.75 mg/ml); the inhibitor NAC was added to wells treated with 0.75 mg/ml PS-NPs, PD98059, and TTM. After 24 h, cell viability was detected by CCK-8 cell proliferation and cytotoxicity kit (Meilunbio, China); absorbance was detected at 450 nm using an enzyme marker, and cell viability was calculated.

Morris water maze

The test was performed in a 120 cm diameter, 50 cm high pool containing water at 23±1 °C. Titanium dioxide was added to the water to render it opaque; the pool was divided into quadrants (I, II, III, and IV); a transparent circular platform (8 cm diameter) was placed in quadrant III. For the first 5 d, mice were trained to locate the platform, and the time taken to swim to and find it within 60 s was recorded; The platform was removed on day 7, and the time taken to locate its historical position within 60 s was recorded. The number of times that mice traversed the historical position of the platform from the opposite quadrant of the target quadrant (quadrant III) and the time were also recorded. All trials were video-recorded, graphically counted, and analyzed using GraphPad Prism version 9.5.1.

Y maze

The spontaneous alternation Y-maze can be used to assess short-term memory in mice. Mice began to explore from the central position and had free access to the three arms for 10 min. The sequence in which the mice entered the arms was recorded, enabling calculation of the spontaneous alternation rate. Graphical statistics and analyses were performed using GraphPad Prism version 9.5.1. All experiments were video recorded.

Novel object recognition

The novel object recognition test was performed in a white opaque cube (40 × 40 × 40 cm) for three consecutive days. On day 1, mice were adapted freely for 6 min. On day 2, two identical objects were placed into the box and mice explored them freely for 5 min. On day 3, one of the objects was replaced with a different rectangle and mice

were permitted to explore freely for 5 min. The time that mice spent sniffing each object was recorded by camera: TN indicates the time spent by the mice on the new object during the test phase, TF indicates the time spent by mice on familiar objects during the test phase. Preference indices (Preference indices = TN/(TN + TF)) were calculated to measure memory capacity.

H&E staining

After 4% paraformaldehyde fixation of brain tissue for 24–48 h, routine dehydration was performed. Paraffin-embedded sections (2 μm) thick were prepared, stained with H&E, and neuron morphology was observed by light microscopy.

Nissl staining

After tissue fixation and dehydration, sections were prepared and stained in 1% aqueous toluene blue. Sections were then differentiated using 70% and 95% alcohol and dehydrated with anhydrous ethanol. Neuron morphology were observed by light microscopy. The number of normal neurons in three distinct brain sections per mice was quantified using ImageJ software, and the mean value was calculated for statistical analysis.

Table 1 Experimental qRT-PCR primer sequences

Genes	Description	Primer sequence (5′-3′)
FDX1(M)	F	TAACAGTCCACTTCAAGAACCGA
	R	CACAACATCTAGCAGAGAGTCG
FDX1(H)	F	TTCAACCTGTCACCTCATCTTTG
	R	TGCCAGATCGAGCATGTCATT
LIAS(M)	F	CCTGGGGTCCCGGATATTTG
	R	GAAGGTCTGGTCCATTATGCAA
LIAS(H)	F	CAGCCCAGTCAGACCGTTAAG
	R	TTTCTGGCGTTTTAGGTTTCCT
DLAT(M)	F	CTTTAGCCTCCAAAGCGAGAG
	R	AGATTGTAAATGTTCCACCCTGG
DLAT(H)	F	CGGAACTCCACGAGTGACC
	R	CCCCGCCATACCCTGTAGT
DLST(M)	F	GGAACTGCCCTCTAGGGAGA
	R	GACGCTACCACTGTTAATGACC
DLST(H)	F	GAACTGCCCTCTAGGGAGAC
	R	AACCTTCCTGCTGTTAGGGTA
HSP70(M)	F	GAGATCGACTCTCTGTTCGAGG
	R	GCCCGTTGAAGAAGTCCTG
HSP70(H)	F	TTGGACGGAAATTCGAGGATG
	R	AAATAGGCCGGGACCGTTATG
SLC31A1(H)	F	GGGGATGAGCTATATGGACTCC
	R	TCACCAAACCGGAAAACAGTAG
ERK(M)	F	ATCTCAACAAAGTTCGAGTTGC
	R	GTCTGAAGCGCAGTAAGATTTT
JNK(M)	F	AAACAGGCCTAAATACGCTGGA
	R	GACGGCTGCCCTCTTATGAC
P38(M)	F	TGACCCTTATGACCAGTCCTTT
	R	GTCAGGCTCTTCCACTCATCTAT

qRT-PCR

Total RNA was extracted from the mice prefrontal cortex (PFC) or collected SH-SY5Y cells for reverse transcription using tissue lysate TRIzol Reagent (Invitrogen, USA). Genes of interest were subjected to SYBR dye (Biosharp, China) and Bio-Rad CFX Reaction System following manufacturer protocols. qPCR, and relevant primer sequences are listed in Table 1.

Western blot analysis

Mice PFC samples or SH-SY5Y cells were lysed in a mixture containing RIPA lysate (strong), 1% protein inhibitor, and 2% phosphatase inhibitor. The supernatant was collected after centrifugation. Protein concentration was determined using the BCA Protein Assay Kit (Beyotime, China), and 30 μg proteins were loaded into SDS-PAGE for separation, then transferred to a PVDF membrane and incubated with corresponding primary antibodies (from ABclonal, China: ERK (1: 1000, A4782), phospho-ERK (1:1000, AP0974), FDX1 (1:1000, A20859), DLAT (1:1000, A8814), HSP70 (1:10000, A23457), and Tublin (1:10000, AC007); from Proteintech, China: LIAS (1:1000, 11577-1-AP); and from Abcam, USA: Anti-Lipoic Acid (1:1000, ab58724). The primary antibody was incubated for 12–16 h, then washed and incubated with anti-rabbit antibody (1:5000, A0208, Beyotime, China) for 1 h at 37 °C. Bands were visualized using an ECL Kit (BL520A, Biosharp, China), and their intensity was further analyzed using Image J software.

Immunohistochemistry analyses

Brain tissues were fixed and embedded in paraffin, sectioned, then deparaffinized to water, followed by antigen repair and closure. Sections were incubated with nuclear factor erythroid 2-related factor 2 (Nrf2, 1:200, Bioss) overnight at 4 °C; then, after rinsing with TBST, sections were incubated dropwise with goat anti-rabbit IgG secondary antibody for 45 min at 37 °C. Freshly prepared DAB (1:20, Fuzhou Maisin) was added dropwise. Nuclei were stained with hematoxylin, and sections were observed by light microscopy, and imaged. The number of positive cells within a fixed area of three distinct brain sections per mice was quantified using ImageJ software, and the mean value was calculated for statistical analysis.

Immunofluorescence staining (IF)

Brain tissues were fixed, sectioned, then deparaffinized to water, followed by antigen repair with ethylenediaminetetraacetic acid (EDTA) buffer. Then 10% donkey serum was added dropwise, sections were blocked at 37 °C for 30 min, then incubated in primary antibody DLAT (1:100, PTG) diluted in TBST at 4 °C overnight. Sections were then incubated with secondary antibody Alexa Fluor 488 donkey anti-rabbit lgG (H + L) (1:400,

ThermoFisher) for 45 min at 37 °C. Nuclei were stained using DAPI working solution for 5 min away from light, then sealed, observed by light microscopy, and imaged. The relative fluorescence intensity of DLAT in a fixed area of three distinct brain sections per mice was quantified using ImageJ software, and the mean value was calculated for statistical analysis.

RNA-sequencing

Mouse PFC tissues were removed and total RNA was extracted using TRIzol reagent. Genomic DNA was removed by DNase I (TaKaRa). RNA quality was determined by 2100 Bioanalyser (Agilent). Libraries were prepared using the TruSeqTM RNA Sample Preparation Kit from Illumina (San Diego, CA).

Transmission electron microscopy

Brain tissue or SH-SY5Y cell samples were fixed with 2.5% glutaraldehyde immediately after collection, dehydrated with gradient ethanol at room temperature, and tissues were embedded to make 60–80 nm sections by ultrathin microtome (Leica UC7, Leica). Sections were stained with uranyl acetate and lead citrate, and the morphology of mitochondria in the PFC of mice and SH-SY5Y cells, as well as the morphology of synapses in the mice PFC, were observed using a transmission electron microscope (TEM; HT7800/HT7700, Hitachi). The number of synapses and the thickness of the postsynaptic density (PSD) within a fixed area of three distinct brain sections per mice were further quantified using ImageJ software, and their mean values were calculated for statistical analysis.

Detection of copper and cuprous content

Tissue copper and cellular cuprous content determination kits were purchased from Elabscience (China). Brain tissue and cell samples were collected by adding saline homogenate, and centrifuged. The supernatant was collected and assayed according to manufacturer protocols. Copper content was detected by 580 nm absorbance using an ordinary enzyme marker; protein concentration was determined by bicinchoninic acid assay; sub-copper content was detected by fluorescence enzyme marker using fluorescence values at excitation wavelength 395 nm and emission wavelength 480 nm in each well.

Measurement of superoxide dismutase and glutathione peroxidase

Protein concentrations were determined using a BCA protein concentration assay kit (Beyotime, China). Superoxide dismutase (SOD) (Beyotime, China), and glutathione (GSH) (Beyotime, China) activities were determined by assay kit following manufacturer instructions.

Statistical analysis

All results are from at least three replicate experiments; data have been analyzed using GraphPad Prism 9.5.1 software, with values expressed as mean ± SEM. Differences between the two groups were evaluated using Student's t-tests; multiple comparisons were performed by one-way ANOVA followed by Tukey's test. P value of < 0.05 was considered statistically significant.

Results

Exposure to polystyrene nanoplastics induces cognitive dysfunction in mice, which can be mitigated by NAC treatment

Scanning electron microscopy revealed PS-NPs to be sub-spherical, well dispersed, and of appropriate size. Their zeta potential in water was −19.4 ± 5.91 mV; particle size was 65.29 nm (Fig.S1). PS-NPs exposure has been shown to induce adverse effects, including oxidative stress, behavioral alterations, and neurotoxicity. In recent years, NAC has garnered increasing attention as a potential therapeutic agent for neurological disorders. To investigate the effects of PS-NPs on cognitive function in C57BL/6 mice and the therapeutic potential of NAC, mice were administered 12.5 mg/kg PS-NPs via oral gavage and provided drinking water containing 2 g/L NAC for 30 days. Cognitive function was assessed using the Novel object recognition test, Y-maze test, and Morris water maze test.

Initially, the NOR test was conducted. The first phase, the habituation phase (Day 31), involved placing mice in an empty arena for free exploration, with their movement trajectories recorded. During this phase, total distance traveled was quantitatively analyzed using a video tracking system. Statistical analysis revealed that all experimental groups exhibited normal exploratory behavior, with no significant differences in locomotor activity between groups ($p > 0.05$). These findings indicate that the experimental mice met the baseline requirements for behavioral testing and rule out potential confounding effects of locomotor differences on subsequent cognitive assessments. In the new-object recognition experiment (Day 33), the preference index for new objects in the NPS treatment was significantly lower than in the control, while that for the NPS + NAC treatment was significantly higher. No significant difference was observed between control and NAC, and NPS + NAC treatments. In the Y-maze experiment, after co-treatment with NPS and NAC, the decrease in alternation rate because of PS-NPs exposure was significantly alleviated. In the water-maze experiment, one-way ANOVA was performed on escape latency and swimming speed during the first five days. On day 39, a significant group difference was observed in escape latency ($F(3, 24) = 4$, $p = 0.0166$). Post-hoc Tukey's tests revealed that the NPS group exhibited significantly

longer escape latencies compared to the control group ($p < 0.05$), while the NPS + NAC groups showed significantly reduced latencies ($p < 0.05$). No significant differences in swimming speed were observed among groups across the first five days. On day 41, the number of platform crossings and the time spent on the platform were significantly lower in the NPS-exposed group compared to the control and NPS + NAC groups. From the results of behavioral experiments, it was found that NAC effectively mitigates the cognitive deficits induced by exposure to PS-NPs (See Fig. 1).

NAC can ameliorate neuropathological damage in PFC brain regions induced in mice after PS-NPs exposure

To evaluate whether NAC could mitigate the effects of PS-NPs exposure on PFC brain morphology, we performed H&E and Nissl staining. Neurons in the control treatment were structurally normal, well-organized, and densely packed, whereas their numbers in the NPS treatment were significantly reduced, and a decrease in numbers of Nissl bodies was apparent. There was a significant increase in the number of normal neurons and Nissl bodies in the NPS + NAC treatment compared with the NPS treatment. TEM also revealed significant reductions in numbers of synapses and postsynaptic density (PSD) thickness in the NPS treatment compared with the control; however, both the number of synapses and PSD thickness were significantly greater in the NPS + NAC treatment than in the NPS treatment. These findings suggest that NAC may improve pathological changes in the PFC region of the mice brain (See Fig. 2).

Effect of PS-NPs on the transcriptome of the PFC region of mice brain tissue

To elucidate the mechanism of PS-NPs-induced neurotoxicity, we performed RNA-seq analysis on the PFC of mice treated with 12.5 mg/kg PS-NPs. Following comparison and quantification of read segments, principal component analysis was performed. Each ellipse in the Venn diagram represents differentially expressed genes (DEGs) in control and PS-NPs-treatments, with the overlap indicating shared DEGs. A total of 1019 DEGs were identified in the NPs-treated samples, of which 620 transcripts were up-regulated and 399 transcripts were

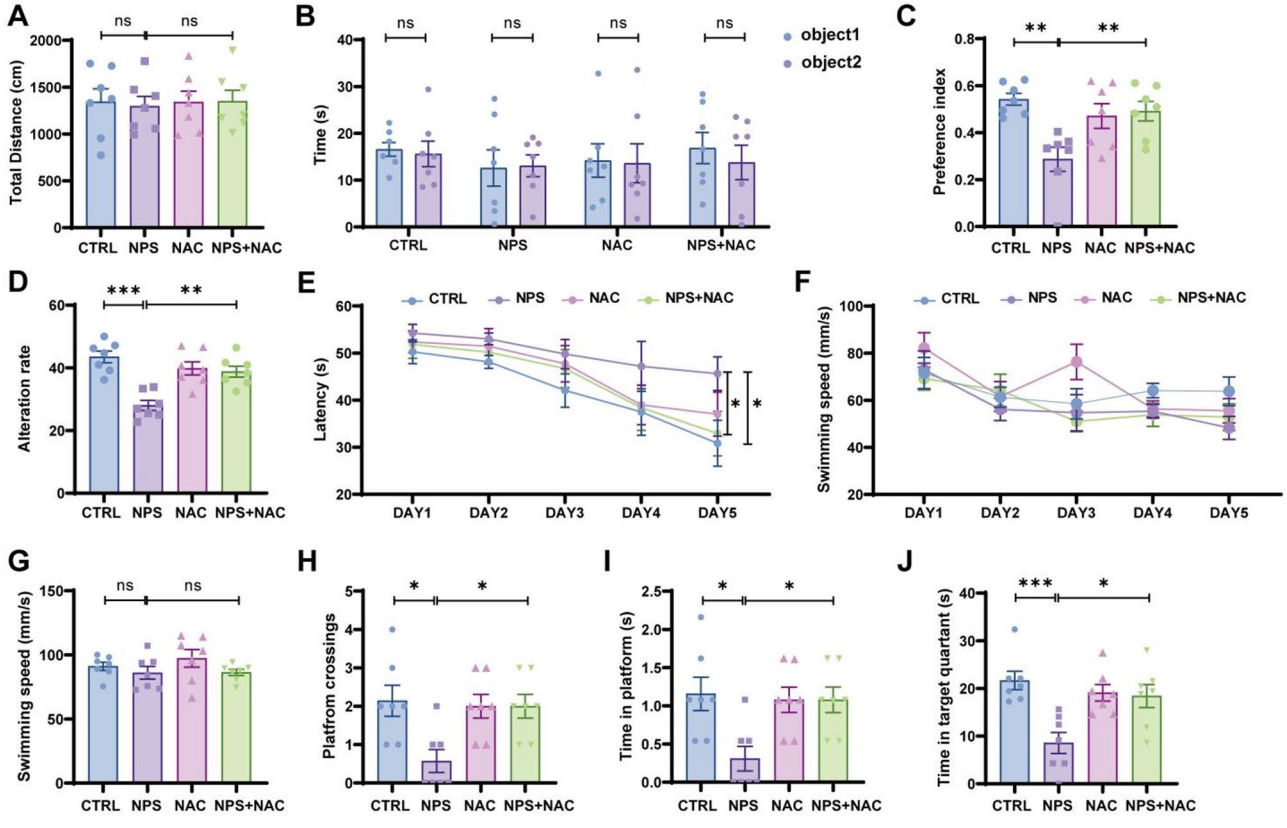

Fig. 1 Exposure to polystyrene nanoplastics induces cognitive dysfunction in mice, which can be mitigated by NAC treatment. (**A**) Total distance traveled by the mice in the empty box. (**B**) Time spent exploring identical objects on day 2 of the new-object recognition experiment. (**C**) Preference index analysis for new-object recognition. (**D**) Alternation rates for mice in the Y maze. (**E**) Avoidance latency for days 1–5. (**F**) Swimming speed for days 1–5. (**G**) Swimming speed for day 7. (**H**-**J**) Statistical graphs of the number of times they traversed the hidden platforms and stayed there, as well as the time they stayed in the quadrant where the hidden platforms were located on day 7. Data expressed as mean ± SEM, one-way ANOVA followed by Tukey's test, $^{*}p < 0.05$, $^{**}p < 0.01$, $^{***}p < 0.001$ vs. Control. $N = 7$ mice per group

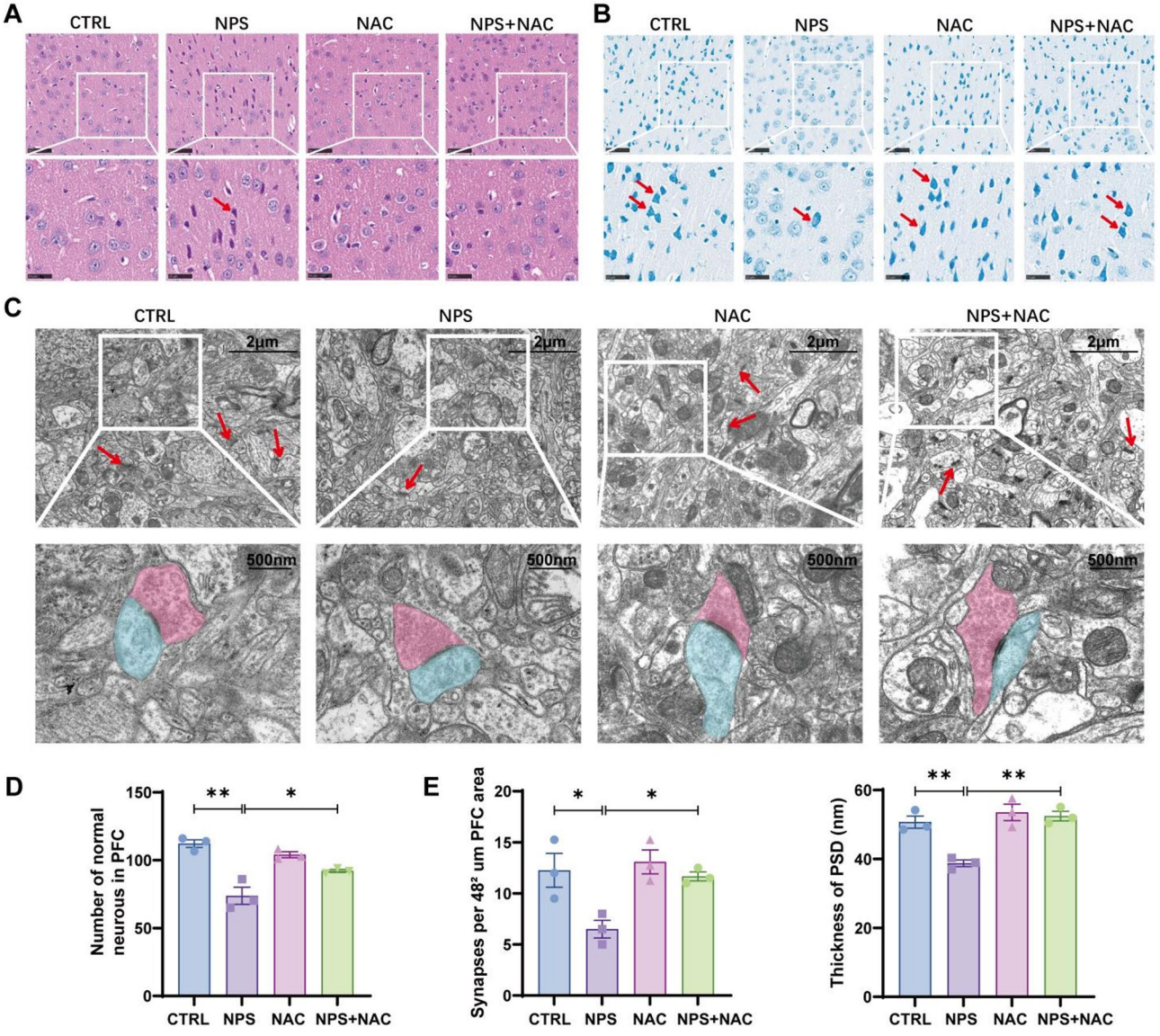

Fig. 2 NAC can ameliorate neuropathological damage in PFC brain regions induced in mice after PS-NPs exposure (**A**) H&E staining of mice brain sections after treatment with PS-NPs; red arrows indicate degenerate neuron. (**B**) Nissl staining of mice brain sections. (**C**) TEM of synaptic structures: representative diagrams and magnified display images of individual synapses. Red arrows indicate representative synapses. (**D**) Quantification of normal cells in PFC. $N = 3$ mice per group. (**E**) Results of statistical analysis of synapse number and PSD thickness. $N = 3$ mice per group. Data expressed as mean ± SEM, one-way ANOVA followed by Tukey's test, $^{*}p < 0.05$, $^{**}p < 0.01$ vs. Control

down-regulated. Genes were enriched in multiple KEGG pathways, with the MAPK signaling pathway in the top five. We hypothesized that regulation of the MAPK signaling pathway and oxidative stress may be the primary pathways contributing to neuronal damage in mice exposed to PS-NPs. We further assessed the expression of genes related to the MAPK pathway at the transcriptional level, revealing mRNA levels of ERK were significantly increased in the NPs-exposed treatment compared with the control, suggesting activation of the MAPK signaling pathway following PS-NPs exposure (See Fig. 3).

NAC attenuates PS-NPs exposure-induced oxidative stress and neuronal Cuproptosis in mice

To better understand molecular mechanisms underlying the protective effect of NAC against PS-NPs-induced neuronal injury, we investigated expression levels of oxidative stress indicators (GSH and SOD) following treatment. Levels of both were significantly lower in the NPs treatment compared with the control. In contrast, the NAC treatment effectively reversed the NPs-induced depletion of GSH and SOD. We also assessed changes in Nrf2; immunohistochemistry results revealed its expression to be reduced following exposure to PS-NPs, but for

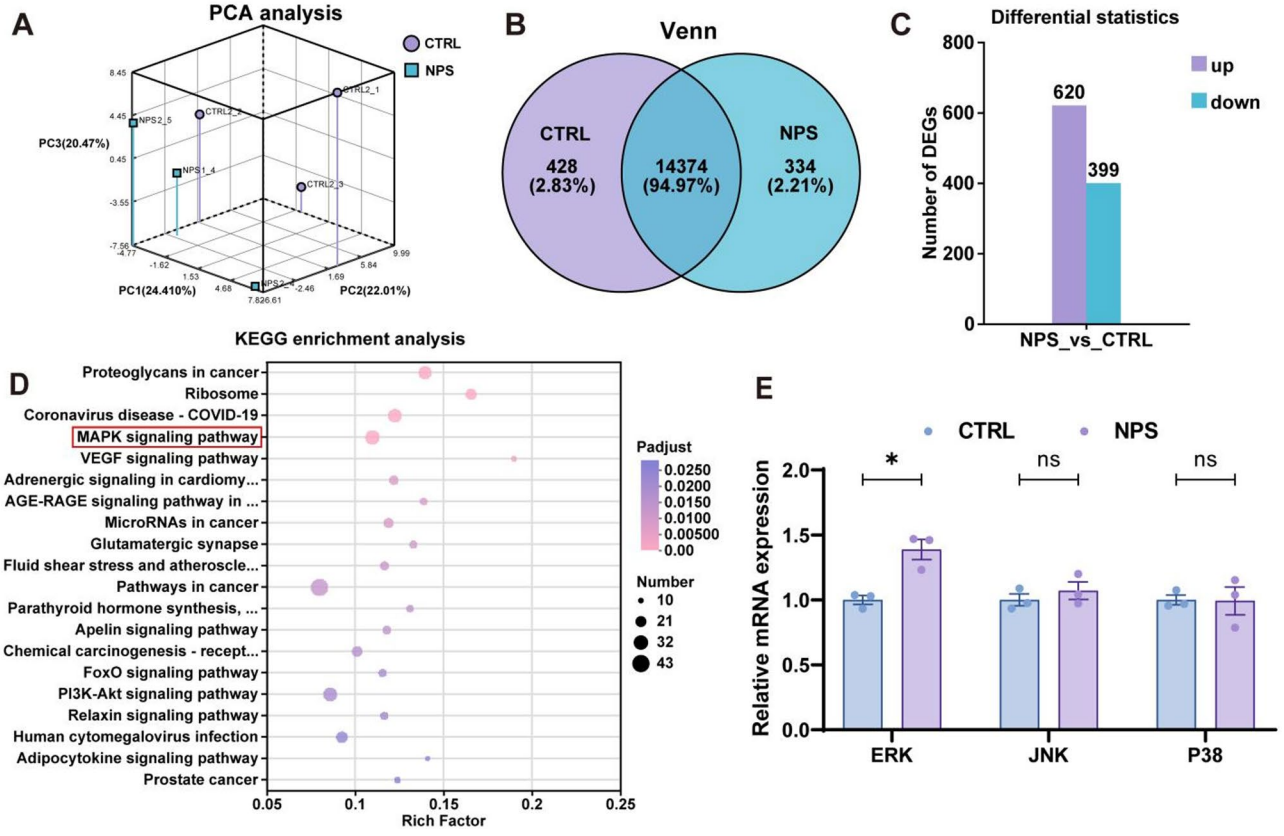

Fig. 3 Effect of PS-NPs on the transcriptome of the PFC region of mouse brain tissue. (**A**) Inter-sample PCA analysis. (**B**) Inter-sample Venn diagram. (**C**) Histogram of significantly induced (red) or repressed (blue) genes after 30 d PS-NPs exposure. (**D**) KEGG enrichment analysis. (**E**) qRT-PCR to detect changes in MAPK family-related genes at the transcriptional level. The data was expressed as the mean ± SEM. *$p < 0.05$ vs. Control. $N = 3$ mice per group

levels to increase significantly following NAC treatment. These findings suggest that NAC can effectively mitigate oxidative stress induced by PS-NPs exposure. Additionally, given that oxidative stress activates the ERK–MAPK pathway, we examined protein expression levels of ERK and its phosphorylated forms post-NAC treatment, and found that NAC could reverse ERK phosphorylation (See Fig. 4).

Copper levels in brain tissues were elevated following exposure to PS-NPs, whereas they significantly decreased after co-treatment with NAC. To elucidate the relationship between PS-NPs exposure, cuproptosis, and NAC, we analyzed expressions of FDX1, LIAS, HSP70, and DLAT, and their lipoic acidified protein levels. FDX1 and LIAS are key regulators of copper toxicity; they act as upstream regulators of protein lipid acylation, facilitating aggregation of mitochondrial proteins and loss of Fe-S clusters.Following PS-NPs exposure, expressions of FDX1, LIAS, DLAT, and HSP70 were significantly increased, levels of lipoic acidified DLAT decreased, and the lipoylated protein DLAT was oligomerized compared with the control treatment. These trends were also mitigated by combined treatment with NAC. For further confirmation, we used TEM to observe ultrastructural changes in mitochondria in the mice PFC region. Following exposure to PS-NPs, specific morphological alterations associated with cuproptosis included reduced or absent mitochondrial cristae densities and ruptured mitochondrial membranes. NAC significantly alleviated these changes compared with the PS-NPs treatment. Therefore, exposure to PS-NPs induced neuronal cuproptosis, which was attenuated by NAC (See Fig. 5).

NAC protects against Cuproptosis induced by PS-NPs in SH-SY5Y cells

After determining these phenomena at the animal level, we validated them at a cellular level. The CCK-8 assay demonstrated that exposure to 0.75 mg/ml PS-NPs for 24 h significantly reduced cell viability in a dose-dependent manner, prompting the selection of this concentration for further experiments. QPCR analysis revealed that 0.75 mg/ml PS-NPs specifically altered the mRNA levels of cuproptosis-related markers (FDX1, LIAS, DLAT, and HSP70) and the copper transporter SLC31A1 (Fig. S2C). Co-treatment with the cuproptosis inhibitor tetrathiomolybdate (TTM, 2 μM) and PS-NPs for 24 h significantly restored cell viability and reduced intracellular Cu^{+} levels (Fig. S2F, G). These findings indicate that PS-NPs

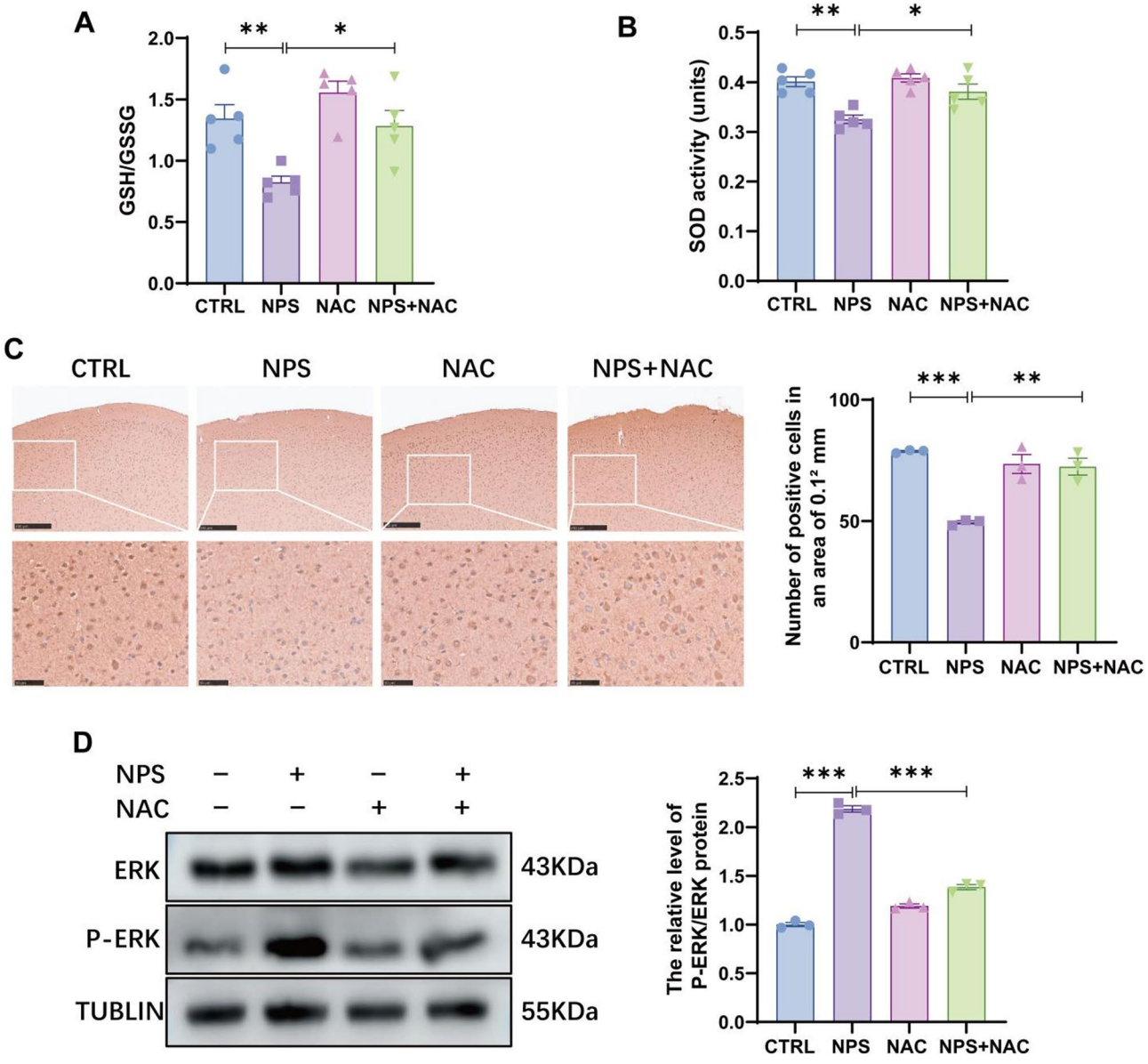

Fig. 4 NAC attenuates PS-NPs exposure-induced oxidative stress and neuronal cuproptosis in mice. (**A**-**B**) GSH and SOD levels. $N = 5$ mice per group. (**C**) Nrf2 protein expression and its quantification detected by immunohistochemistry. $N = 3$ mice per group. (**D**) Protein expression level of ERK and its quantification. $N = 3$ mice per group. Data expressed as mean ± SEM, one-way ANOVA followed by Tukey's test, $^{*}p < 0.05$, $^{**}p < 0.01$, $^{***}p < 0.001$ vs. Control

exposure induces neuronal damage through cuproptosis. To clarify the protective effect of NAC against cell damage induced by PS-NPs, we assessed cell viability using the CCK-8 assay following a 24-h co-treatment with NAC (5 μM) and PS-NPs (0.75 mg/ml). While cell viability was significantly reduced in the PS-NPs treatment compared with the control, and co-treatment with NAC markedly enhanced cell viability relative to the PS-NPs treatment. We then investigated expression levels of GSH and SOD in SH-SY5Y cells, which were both significantly lower in the PS-NPs treatment compared with the control, while NAC effectively reversed this. Because oxidative stress resulting from PS-NPs exposure can activate the MAPK pathway, we assessed levels of phosphorylated ERK. NAC co-treatment successfully reversed ERK phosphorylation (See Fig. 6).

To examine conditions under which cuproptosis occurred, we measured intracellular Cu^{+} contents. While exposure to PS-NPs converted original Cu^{2+} into toxic Cu^{+} in substantial quantities, NAC co-treatment largely restored Cu^{+} levels. Following PS-NPs exposure, protein levels of markers associated with cuproptosis (FDX1, LIAS, DLAT, and HSP70) were significantly elevated, while lipoic acidified DLAT was lowered; these alterations were reversed with NAC treatment. Additionally, we observed morphological changes in intracellular

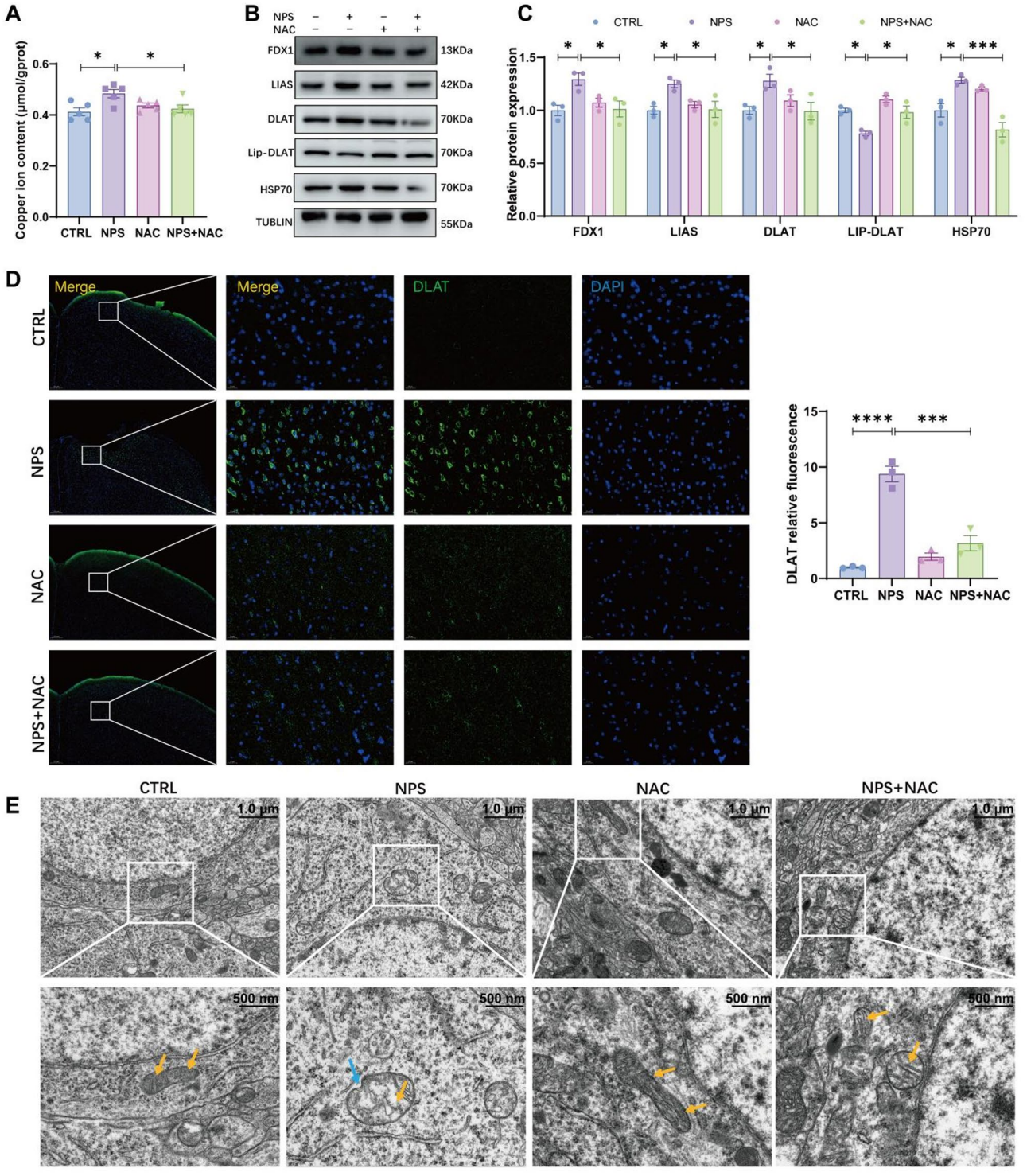

Fig. 5 NAC attenuates PS-NPs exposure-induced oxidative stress and neuronal cuproptosis in mice. (**A**) Copper level in brain tissues. $N = 5$ mice per group. (**B**) Cuproptosis marker protein expression levels. (**C**) Quantification of cuproptosis marker protein levels. $N = 3$ mice per group. (**D**) Representative images of DLAT oligomers detected by immunofluorescence (green, DLAT oligomers; blue, DAPI) and DLAT relative fluorescence intensity. $N = 3$ mice per group. (**E**) TEM images of the PFC region of mouse brain: yellow arrows, reduction or dissolution of mitochondrial cristae; blue arrow, cell membrane rupture. $N = 3$ mice per group. Data expressed as mean ± SEM, one-way ANOVA followed by Tukey's test, $^{*}p < 0.05$, $^{****}p < 0.0001$ vs. Control

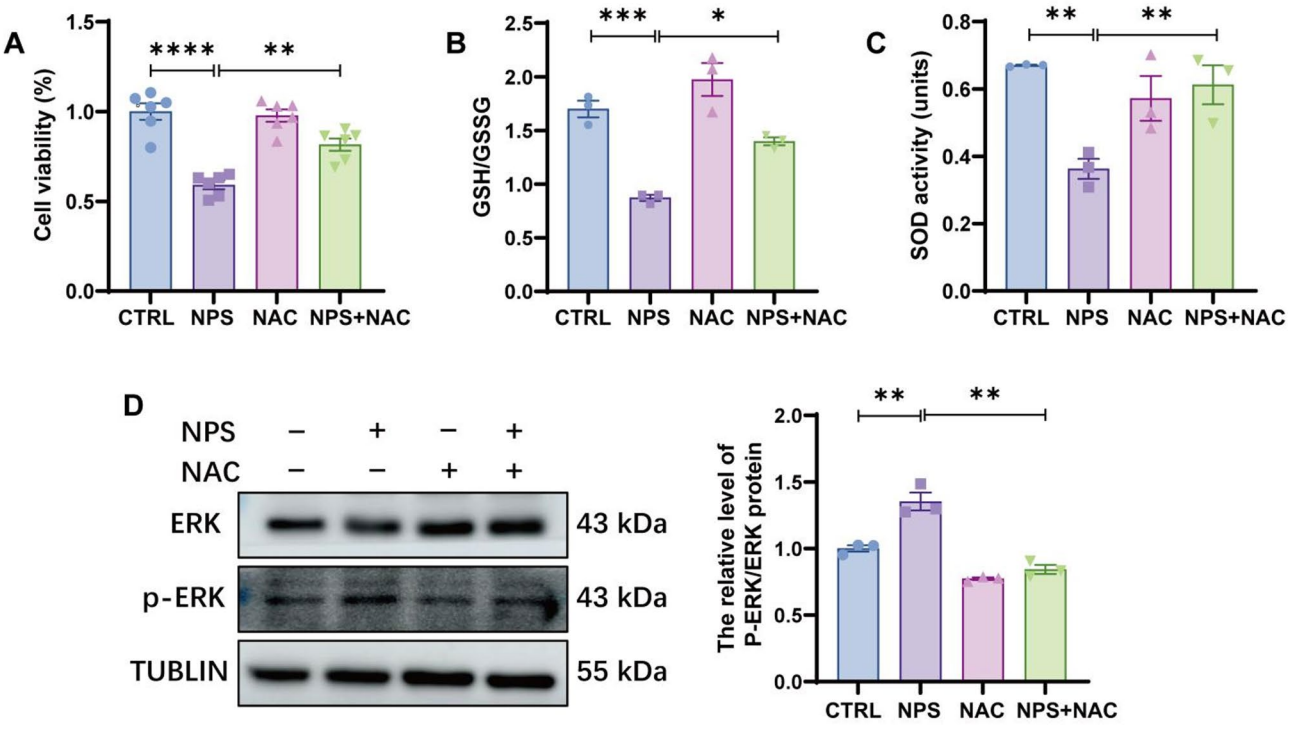

Fig. 6 NAC protects against cuproptosis induced by PS-NPs in SH-SY5Y cells. (**A**) Cell viability detected by CCK-8 after 24 h co-treatment with NAC (5μM). (**B**-**C**) GSH and SOD levels. $N = 3$. (**D**) Protein expression of ERK and its quantification. $N = 3$. Data expressed as mean ± SEM, one-way ANOVA followed by Tukey's test, $^{*}p < 0.05$, $^{**}p < 0.01$, $^{***}p < 0.001$ vs. Control

mitochondria using TEM, which aligned with findings from animal experiments; SH-SY5Y cells in the PS-NPs treatment exhibited morphological alterations consistent with cuproptosis. NAC significantly mitigated these changes when compared with the PS-NPs treatment. In conclusion, NAC effectively attenuated PS-NPs-induced cellular cuproptosis (See Fig. 7).

Inhibition of activated MAPK pathways prevents PS-NPs-induced cellular damage

To explore relationships between the MAPK signaling pathway and cuproptosis, we selected PD98059, a specific inhibitor of ERK. Following co-treatment with PD98059 (5μM) and PS-NPs (0.75 mg/ml) for 24 h, we assessed cell viability using the CCK-8 assay. A significant increase in cell viability was apparent after PD98059 co-treatment compared with the NPS treatment alone. Concurrently, we measured intracellular Cu^{+} levels, and found the elevated cuprous levels following exposure to PS-NPs were significantly reduced after PD98059 co-treatment. Next, we evaluated protein levels of cuproptosis-associated markers. Levels of FDX1, LIAS, DLAT, and HSP70 were all significantly elevated after exposure to PS-NPs, while lipoic acidified DLAT was reduced; these changes were mitigated following PD98059 treatment. Finally, we examined the mitochondria using TEM and report damage to be largely reversed after PD98059 co-treatment. Collectively, these results demonstrate that inhibition of the MAPK pathway, activated by oxidative stress, can suppress PS-NPs-induced cuproptosis (See Fig. 8).

Discussion

Globally, humans ingest 0.1–5 g of plastic per week, which corresponds to an estimated daily dose of 0.05–2.9 mg of NPs in mice [31]. Exposure to high doses of NPs (≥ 500 μg/d) can significantly affect brain function [32]. For instance, administering 100 nm PS-NPs at a dose of 1 mg/d via gavage for 28 d resulted in anxiety and depression [33]. Additionally, exposure to 80 nm PS-NPs at a dosage of 50 mg/kg/d for 7 d impaired learning and memory functions [34]. All nanoparticles < 500 nm can penetrate the mouse brain, leading to neurotoxicity and a spectrum of behavioral changes [35]. While most literature indicates that PS-NP exposure damages mouse hippocampal neurons [36, 37], fewer studies have examined effects on the PFC (considered the highest stage of neural integration, specializing in behavioral representation and production [38]. PFC primary projection neurons (pyramidal neurons) regulate various aspects of behavior, including short- [39] and long-term memory [40], by facilitating memory through cognitive or strategic control of memory-extraction processes within other brain regions [41–43]. Notably, Compared to other brain regions, the frontal cortex exhibits significantly elevated

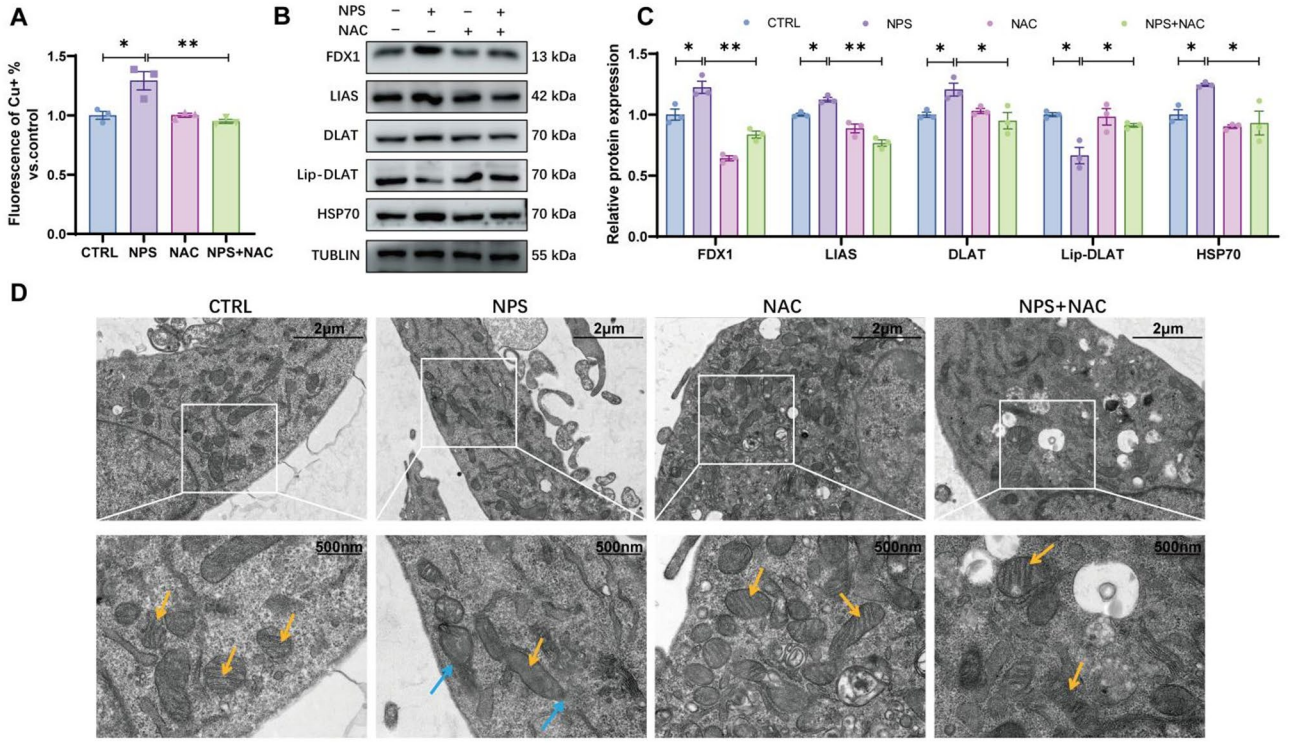

Fig. 7 NAC protects against cuproptosis induced by PS-NPs in SH-SY5Y cells. (**A**) Monovalent copper levels in cells. (**B**-**C**) Protein levels of cuproptosis-related biomarkers in cells and their quantification. (**D**) TEM images of SH-SY5Y cells: yellow arrows, reduction or lysis of mitochondrial cristae; blue arrow, cell membrane rupture. Data expressed as mean ± SEM, one-way ANOVA followed by Tukey's test, $^{*}p < 0.05$, $^{**}p < 0.01$ vs. Control. $N = 3$

concentrations of NPs [44]. We focused on the PFC using a mouse model subjected to 30 days of oral gavage with 60 nm PS-NPs at 12.5 mg/kg/d, a dose selected to model environmentally relevant exposure. Behavioral assessments, including the novel object recognition test, Y-maze, and Morris Water Maze, revealed pronounced deficits in executive function, consistent with PFC impairment [39]. Histological analyses (H&E and Nissl staining) and TEM confirmed PS-NPs-induced neuronal damage in the PFC. In the MWM behavioral assessment, PS-NPs exposure significantly impaired spatial learning and memory in mice ($P < 0.05$), as evidenced by prolonged escape latency and reduced platform crossings, in which this significant behavioral effect may primarily be driven by four animals in the experimental group that never successfully crossed the platform, exhibiting longer escape latencies and reduced time spent in the platform quadrant, suggesting potential subpopulation differences in behavioral performance. This subpopulation effect may partly be attributed to variations in individual stress responses during the experiment or uneven distribution of PS-NPs in the PFC. Crucially, we report, for the first time, hallmark features of cuproptosis in the PFC of PS-NPs-exposed mice, including aberrant aggregation of lipoylated proteins, characteristic changes in key cuproptosis-related factors, and mitochondrial structural damage. In our preliminary investigations, we observed statistically significant changes in the expression of cuproptosis-related genes in the PFC. Furthermore, we detected cuproptosis following 24 h of exposure to 0.75 mg/ml PS-NPs using the SH-SY5Y in vitro model, which consists of human neuroblastoma cells that resemble proximal neurons. TTM, a known cuproptosis inhibitor, effectively binds excess copper ions and can mitigate cytotoxicity associated with elevated copper levels [45]. Our findings indicate that co-treatment with TTM can alleviate cuproptosis induced by PS-NPs exposure. We demonstrate that exposure to PS-NPs can induce neuronal cuproptosis, subsequently influencing mouse behavior.

Cuproptosis can be induced by increasing levels of exogenous copper or by introducing copper carriers [46–48]. However, few studies have examined stimulation by external factors that convert a greater proportion of the body's original Cu^{2+} to Cu^{+}, inducing cuproptosis. The underlying mechanisms remain even more poorly understood, and no research has addressed whether cuproptosis occurs following exposure to PS-NPs. When intracellular copper concentrations surpass the threshold necessary to maintain homeostasis, they target and bind to lipoylated components of the TCA cycle and cause abnormal aggregation of lipoylated proteins (a hallmark

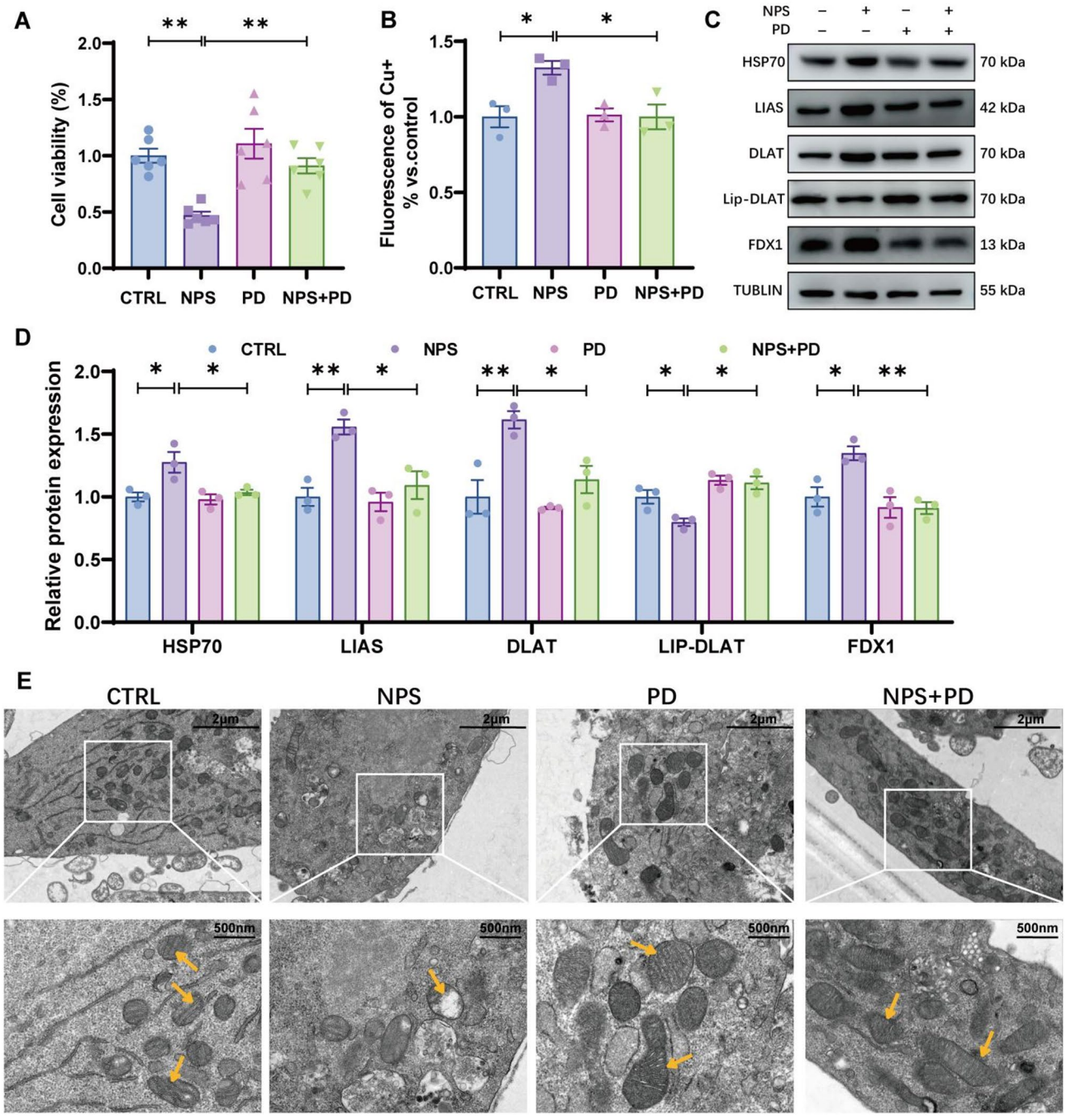

Fig. 8 Inhibition of activated MAPK pathways prevents PS-NPs-induced cellular damage. (**A**) Cell viability detected by CCK-8 after adding PD98059 (5μM) for 24 h co-treatment. (**B**) Monovalent copper levels in cells. (**C**-**D**) Protein levels of cuproptosis-related biomarkers in cells and their quantification. (**E**) TEM images of SH-SY5Y cells after PD98059 co-treatment: yellow arrows, reduction or lysis of mitochondrial cristae. Data expressed as mean ± SEM, one-way ANOVA followed by Tukey's test, $^{*}p < 0.05$, $^{**}p < 0.01$ vs. Control. $N = 3$

of cuproptosis). Protein lipoylation, a post-translational modification predominantly found in enzymes involved in mitochondrial metabolic pathways such as the TCA cycle is coordinated with copper overload by FDX1-a key regulator of cuproptosis and an upstream regulator of protein lipid acylation [49]. FDX1 also directly interacts with LIAS to enhance production of the lipoicyl moiety, which requires lipoicyl transferase for transfer to target proteins such as DLAT [50], ultimately causing cuproptosis. We demonstrate that copper levels were significantly upregulated in PFC and SH-SY5Y cells. Additionally, transcript levels of the copper transporter SLC31A1 were elevated, DLAT was abnormally aggregated, and FDX1 was upregulated, contributing to increased expression

of HSP70. Because cuproptosis disrupts the TCA cycle, mitochondria (the site of this process) are the main targets [51]. We observed mitochondrial damage following exposure to PS-NPs, characterized by formation of vacuoles and mitochondrial cristae lysis.

Oxidative stress induces cell death [52]. GSH and SOD are two important markers of oxidative stress. GSH plays an important role in antioxidant defense and in preventing intracellular oxidative damage [53], and is closely associated with the onset of cuproptosis [54]. The role of GSH in cuproptosis is primarily attributed to its chelating effect on copper ions. By binding to these ions, GSH reduces the concentration of free copper, thereby inhibiting the occurrence of copper-mediated cell death [55]. Upregulation of GSH expression also can mitigate copper toxicity by functioning as a sulfhydryl-containing copper chelator [56, 57]. Concurrently, in the cytoplasm, SOD 1 serves as a copper chaperone, delivering copper to specific proteins to detoxify ROS and maintain copper homeostasis [58]. We report levels of GSH and SOD to be downregulated in vivo and *vitro*, reinforcing that cuproptosis occurred. NAC is a precursor that facilitates biosynthesis of L-cysteine from GSH [59], mitigating the cytotoxic effects of certain copper carriers [60]. Consequently, we investigated the relationship between oxidative stress and cuproptosis, using NAC as an inhibitor. NAC was administered orally to enable its penetration into mouse brain tissues via the blood–brain barrier, thereby inhibiting oxidative stress. NAC treatment effectively alleviated cuproptosis caused by PS-NPs in both animal models and cell cultures. Furthermore, pathological damage in the PFC was significantly reduced in the NAC + PS-NPs treatment. NAC treatment also improved cognitive deficits in mice. These findings suggest that PS-NPs induce neuronal cuproptosis through via oxidative stress, which then contribute to cognitive impairment in mice. ROS-generated oxidative stress is linked to activation of the ERK pathway [61], and ERK is important in cellular signaling; sustained activation of ERK, followed by its translocation to the nucleus, promotes neuronal cell death [62]. DSF@CuO gel inhibited the cancer stemness pathway by activating the JNK/p38 MAPK pathway, effectively inducing cuproptosis in hepatocellular carcinoma cells [63]. However, the potential association of the ERK–MAPK pathway with cuproptosis and its underlying mechanisms remains underexplored. Consequently, we used the ERK-specific inhibitor PD98059 in SH-SY5Y cells. Co-treatment of PD98059 with PS-NPs significantly rescued cell viability, and largely mitigated changes in cuproptosis-related markers induced by PS-NPs. Thus, we conjecture that inhibition of the oxidative stress-activated ERK–MAPK pathway offers protection against PS-NPs-induced cellular injury.

PS-NPs have the ability to cross the blood-brain barrier and accumulate in the brain, potentially leading to neurotoxic responses. However, their specific role in inducing cuproptosis and causing damage to the central nervous system remains poorly understood. In this study, we present the novel finding that exposure to 60 nm PS-NPs induces cognitive dysfunction by triggering cuproptosis. Nonetheless, methodological limitations hinder the acquisition and quantification of environmentally degraded polystyrene particles. Consequently, synthetic polystyrene nanoparticles are predominantly utilized in this study to assess their potential toxic effects. The collection and extraction of environmentally degraded nanoplastics of various compositions, as well as an investigation into their similar toxicity, warrant further exploration.

Conclusions

This study provides novel insights into the neurotoxicity of PS-NPs. Our findings indicate that oxidative stress induced by PS-NPs may activate the ERK-MAPK pathway, potentially facilitating the conversion of Cu2 + to toxic Cu+, thereby promoting neuronal cuproptosis. This process is associated with ultrastructural mitochondrial damage and deficits in learning and memory. These results present a new perspective on the role of neuronal cuproptosis in PS-NPs-mediated cognitive impairment. Furthermore, we demonstrate that NAC may mitigate PS-NPs-induced toxicity, suggesting a potential protective role. These preliminary findings enhance our understanding of the neurological effects of PS-NPs exposure, and future studies will aim to validate these mechanisms across multiple brain regions and assess their relevance to human health.

Supplementary Information

The online version contains supplementary material available at https://doi.org/10.1186/s12989-025-00633-w.

Supplementary Material 1

Acknowledgements

The authors would like to express their gratitude to EditSprings (https://www.editsprings.cn) for the expert linguistic services provided.

Author contributions

Yinuo Chen: Methodology, Investigation, Formal analysis, Writing-Original Draft, Writing-Reviewing and Editing. Yiyang Nan: Methodology, Investigation, Formal analysis, Writing-Original Draft. Lang Xu: Conceptualization, Methodology, Formal analysis, Writing-Original Draft. Anqi Dai: Methodology, Investigation. Rosa Maria Martinez Orteg: Writing-Reviewing and Editing. Mantong Ma: Formal analysis, Writing-Original Draft. Yan Zeng: Conceptualization, Resources, Software, Supervision, Writing - original draft, Writing-Reviewing and Editing. Jinquan Li: Conceptualization, Methodology, Formal analysis, Writing-Reviewing and Editing, Supervision, Project administration, Funding acquisition. All authors reviewed the manuscript.

Funding
This work was supported by grants Science and Technology Innovation 2030 Major Projects (2022ZD0211600), Natural Science Foundation of Hubei Province of China (2024FB685), "The 14th Five year Plan" Hubei provincial advantaged characteristic disciplines (groups) project of Wuhan University of Science and Technology (2023C0106), the Outstanding Young and Middle-aged Technology Innovation Team Project of the Hubei Provincial Department of Education (T2022004) and College Students Innovative Entrepreneurial Training Plan Program (S202310488174).

Data availability
No datasets were generated or analysed during the current study.

Declarations

Ethical approval
All animal experimental procedures were approved by the Ethics Committee for Animal Experiments of the Wuhan University of Science and Technology (Issue number: WUST-2022075).

Competing interests
The authors declare no competing interests.

Author details
[1]Hubei Provincial Clinical Research Center for Alzheimer's Disease, Brain Science and Advanced Technology Institute, School of Medicine, Wuhan University of Science and Technology, Wuhan 430081, China
[2]Hubei Province Key Laboratory of Occupational Hazard Identification and Control, Wuhan University of Science and Technology, Wuhan, China
[3]Sukuta Bojang Clinic, Banjul, The Gambia
[4]School of Medicine, Wuhan University, Wuhan, China

Received: 5 February 2025 / Accepted: 12 May 2025
Published online: 20 May 2025

References

1. Senathirajah K, Attwood S, Bhagwat G, Carbery M, Wilson S, Palanisami T. Estimation of the mass of microplastics ingested - A pivotal first step towards human health risk assessment. J Hazard Mater. 2021. https://doi.org/10.1016/j.jhazmat.2020.124004. 404 Pt B:124004. https://www.ncbi.nlm.nih.gov/pubmed/33130380.
2. Zhu Y, Che R, Zong X, Wang J, Li J, Zhang C, et al. A comprehensive review on the source, ingestion route, attachment and toxicity of microplastics/nanoplastics in human systems. J Environ Manage. 2024;352:120039. https://doi.org/10.1016/j.jenvman.2024.120039. https://www.ncbi.nlm.nih.gov/pubmed/38218169.
3. Kopatz V, Wen K, Kovacs T, Keimowitz AS, Pichler V, Widder J, et al. Micro- and nanoplastics breach the Blood-Brain barrier (BBB): biomolecular Corona's role revealed. Nanomaterials (Basel). 2023;13:8. https://doi.org/10.3390/nano13081404. https://www.ncbi.nlm.nih.gov/pubmed/37110989.
4. Garcia MM, Romero AS, Merkley SD, Meyer-Hagen JL, Forbes C, Hayek EE, et al. In vivo tissue distribution of polystyrene or mixed polymer microspheres and metabolomic analysis after oral exposure in mice. Environ Health Perspect. 2024;132 4:47005. https://doi.org/10.1289/EHP13435. https://www.ncbi.nlm.nih.gov/pubmed/38598326.
5. Prust M, Meijer J, Westerink RHS. The plastic brain: neurotoxicity of micro- and nanoplastics. Part Fibre Toxicol. 2020;17(1):24. https://doi.org/10.1186/s12989-020-00358-y. https://www.ncbi.nlm.nih.gov/pubmed/32513186.
6. Shan S, Zhang Y, Zhao H, Zeng T, Zhao X. Polystyrene nanoplastics penetrate across the blood-brain barrier and induce activation of microglia in the brain of mice. Chemosphere. 2022;298:134261. https://doi.org/10.1016/j.chemosphere.2022.134261. https://www.ncbi.nlm.nih.gov/pubmed/35302003.
7. Han SW, Choi J, Ryu KY. Recent progress and future directions of the research on nanoplastic-induced neurotoxicity. Neural Regen Res. 2024;19 2:331–5. https://doi.org/10.4103/1673-5374.379016. https://www.ncbi.nlm.nih.gov/pubmed/37488886.
8. Jeong A, Park SJ, Lee EJ, Kim KW. Nanoplastics exacerbate Parkinson's disease symptoms in C. elegans and human cells. J Hazard Mater. 2024;465:133289. https://doi.org/10.1016/j.jhazmat.2023.133289. https://www.ncbi.nlm.nih.gov/pubmed/38157817.
9. Schroter L, Jentsch L, Maglioni S, Munoz-Juan A, Wahle T, Limke A, et al. A multisystemic approach revealed aminated polystyrene Nanoparticles-Induced neurotoxicity. Small. 2024;20 10:e2302907. https://doi.org/10.1002/smll.202302907. https://www.ncbi.nlm.nih.gov/pubmed/37899301.
10. Choudhury A, Simnani FZ, Singh D, Patel P, Sinha A, Nandi A, et al. Atmospheric microplastic and nanoplastic: the toxicological paradigm on the cellular system. Ecotoxicol Environ Saf. 2023;259:115018. https://doi.org/10.1016/j.ecoenv.2023.115018. https://www.ncbi.nlm.nih.gov/pubmed/37216859.
11. Paing YMM, Eom Y, Song GB, Kim B, Choi MG, Hong S, et al. Neurotoxic effects of polystyrene nanoplastics on memory and microglial activation: insights from in vivo and in vitro studies. Sci Total Environ. 2024;924:171681. https://doi.org/10.1016/j.scitotenv.2024.171681. https://www.ncbi.nlm.nih.gov/pubmed/38490422.
12. Wei S, Ma X, Liang G, He J, Wang J, Chen H, et al. The role of circHmbox1(3,4) in ferroptosis-mediated cognitive impairments induced by manganese. J Hazard Mater. 2024;476:135212. https://doi.org/10.1016/j.jhazmat.2024.135212. https://www.ncbi.nlm.nih.gov/pubmed/39024764.
13. Yang ZJ, Huang SY, Zhong KY, Huang WG, Huang ZH, He TT, et al. Betaine alleviates cognitive impairment induced by homocysteine through attenuating NLRP3-mediated microglial pyroptosis in an m(6)A-YTHDF2-dependent manner. Redox Biol. 2024;69:103026. https://doi.org/10.1016/j.redox.2024.103026. https://www.ncbi.nlm.nih.gov/pubmed/38184996.
14. Li C, Chen X, Du Z, Geng X, Li M, Yang X, et al. Inhibiting ferroptosis in brain microvascular endothelial cells: A potential strategy to mitigate polystyrene nanoplastics–induced blood–brain barrier dysfunction. Environ Res. 2024;250:118506. https://doi.org/10.1016/j.envres.2024.118506. https://www.ncbi.nlm.nih.gov/pubmed/38387496.
15. Lv J, Tan Z, An Z, Xu R, Zhang H, Guo M, et al. Co-exposure to polystyrene nanoplastics and F-53B induces vascular endothelial cell pyroptosis through the NF-kappaB/NLRP3 pathway. J Hazard Mater. 2025;486:137114. https://doi.org/10.1016/j.jhazmat.2025.137114. https://www.ncbi.nlm.nih.gov/pubmed/39764954.
16. Zhang Y, Tian L, Chen J, Liu X, Li K, Liu H, et al. Selective bioaccumulation of polystyrene nanoplastics in fetal rat brain and damage to Myelin development. Ecotoxicol Environ Saf. 2024;278:116393. https://doi.org/10.1016/j.ecoenv.2024.116393. https://www.ncbi.nlm.nih.gov/pubmed/38714083.
17. Li X, Chen X, Gao X. Copper and Cuproptosis: new therapeutic approaches for Alzheimer's disease. Front Aging Neurosci. 2023;15:1300405. https://doi.org/10.3389/fnagi.2023.1300405. https://www.ncbi.nlm.nih.gov/pubmed/38178962.
18. Chen Z, Liu J, Zheng M, Mo M, Hu X, Liu C, et al. TRIM24-DTNBP1-ATP7A mediated astrocyte Cuproptosis in cognition and memory dysfunction caused by Y(2)O(3) NPs. Sci Total Environ. 2024;954:176353. https://doi.org/10.1016/j.scitotenv.2024.176353. https://www.ncbi.nlm.nih.gov/pubmed/39304169.
19. Yang L, Yang P, Lip GYH, Ren J. Copper homeostasis and Cuproptosis in cardiovascular disease therapeutics. Trends Pharmacol Sci. 2023;44 9:573–85. https://doi.org/10.1016/j.tips.2023.07.004. https://www.ncbi.nlm.nih.gov/pubmed/37500296.
20. Huang M, Zhang Y, Liu X. The mechanism of Cuproptosis in Parkinson's disease. Ageing Res Rev. 2024;95:102214. https://doi.org/10.1016/j.arr.2024.102214. https://www.ncbi.nlm.nih.gov/pubmed/38311254.
21. Zhu Z, Song M, Ren J, Liang L, Mao G, Chen M. Copper homeostasis and Cuproptosis in central nervous system diseases. Cell Death Dis. 2024;15 11:850. https://doi.org/10.1038/s41419-024-07206-3. https://www.ncbi.nlm.nih.gov/pubmed/39567497.
22. Zhao Q, Ma L, Chen S, Huang L, She G, Sun Y, et al. Tracking mitochondrial Cu(I) fluctuations through a ratiometric fluorescent probe in AD model cells: towards Understanding how AbetaOs induce mitochondrial Cu(I) dyshomeostasis. Talanta. 2024;271:125716. https://doi.org/10.1016/j.talanta.2024.125716. https://www.ncbi.nlm.nih.gov/pubmed/38301373.
23. Chen L, Min J, Wang F. Copper homeostasis and Cuproptosis in health and disease. Signal Transduct Target Ther. 2022;7(1):378. https://doi.org/10.1038/s41392-022-01229-y. https://www.ncbi.nlm.nih.gov/pubmed/36414625.
24. Averill-Bates D. Reactive oxygen species and cell signaling. Rev Biochim Biophys Acta Mol Cell Res. 2024;1871 2:119573. https://doi.org/10.1016/j.bbamcr.2023.119573. https://www.ncbi.nlm.nih.gov/pubmed/37949302.
25. Ma MM, Zhao J, Liu L, Wu CY. Identification of cuproptosis-related genes in Alzheimer's disease based on bioinformatic analysis. Eur J Med Res. 2024;29. https://doi.org/10.1186/s40001-024-02093-y. 1:495. https://www.ncbi.nlm.nih.gov/pubmed/39396083.

26. Wu Q, Liu C, Liu D, Wang Y, Qi H, Liu X, et al. Polystyrene nanoplastics-induced lung apoptosis and ferroptosis via ROS-dependent Endoplasmic reticulum stress. Sci Total Environ. 2024;912:169260. https://doi.org/10.1016/j.scitotenv.2023.169260. https://www.ncbi.nlm.nih.gov/pubmed/38086481.
27. Xu D, Ma Y, Peng C, Gan Y, Wang Y, Chen Z, et al. Differently surface-labeled polystyrene nanoplastics at an environmentally relevant concentration induced Crohn's ileitis-like features via triggering intestinal epithelial cell necroptosis. Environ Int. 2023;176:107968. https://doi.org/10.1016/j.envint.2023.107968. https://www.ncbi.nlm.nih.gov/pubmed/37201399.
28. Meng X, Ge L, Zhang J, Xue J, Gonzalez-Gil G, Vrouwenvelder JS, et al. Systemic effects of nanoplastics on multi-organ at the environmentally relevant dose: the insights in physiological, histological, and oxidative damages. Sci Total Environ. 2023;892:164687. https://doi.org/10.1016/j.scitotenv.2023.164687. https://www.ncbi.nlm.nih.gov/pubmed/37290651.
29. Nair AB, Jacob S. A simple practice guide for dose conversion between animals and human. J Basic Clin Pharm. 2016;7 2:27–31. https://doi.org/10.4103/0976-0105.177703. https://www.ncbi.nlm.nih.gov/pubmed/27057123.
30. Cheung YT, Lau WK, Yu MS, Lai CS, Yeung SC, So KF, et al. Effects of all-trans-retinoic acid on human SH-SY5Y neuroblastoma as in vitro model in neurotoxicity research. Neurotoxicology. 2009;30. https://doi.org/10.1016/j.neuro.2008.11.001. 1:127– 35; doi:. https://www.ncbi.nlm.nih.gov/pubmed/19056420.
31. Mohamed Nor NH, Kooi M, Diepens NJ, Koelmans AA. Lifetime accumulation of microplastic in children and adults. Environ Sci Technol. 2021;55 8:5084–96. https://doi.org/10.1021/acs.est.0c07384. https://www.ncbi.nlm.nih.gov/pubmed/33724830.
32. Jeong B, Baek JY, Koo J, Park S, Ryu YK, Kim KS, et al. Maternal exposure to polystyrene nanoplastics causes brain abnormalities in progeny. J Hazard Mater. 2022;426:127815. https://doi.org/10.1016/j.jhazmat.2021.127815. https://www.ncbi.nlm.nih.gov/pubmed/34823950.
33. Ma Y, Xu D, Wan Z, Wei Z, Chen Z, Wang Y, et al. Exposure to different surface-modified polystyrene nanoparticles caused anxiety, depression, and social deficit in mice via damaging mitochondria in neurons. Sci Total Environ. 2024;919:170739. https://doi.org/10.1016/j.scitotenv.2024.170739. https://www.ncbi.nlm.nih.gov/pubmed/38340854.
34. Sun M, Zhang M, Di F, Bai W, Sun J, Zhang M, et al. Polystyrene nanoplastics induced learning and memory impairments in mice by damaging the glymphatic system. Ecotoxicol Environ Saf. 2024;284:116874. https://doi.org/10.1016/j.ecoenv.2024.116874. https://www.ncbi.nlm.nih.gov/pubmed/39153278.
35. Jin H, Yang C, Jiang C, Li L, Pan M, Li D, et al. Evaluation of neurotoxicity in BALB/c mice following chronic exposure to polystyrene microplastics. Environ Health Perspect. 2022;130 10:107002. https://doi.org/10.1289/EHP10255. https://www.ncbi.nlm.nih.gov/pubmed/36251724.
36. Lee CW, Hsu LF, Wu IL, Wang YL, Chen WC, Liu YJ, et al. Exposure to polystyrene microplastics impairs hippocampus-dependent learning and memory in mice. J Hazard Mater. 2022;430:128431. https://doi.org/10.1016/j.jhazmat.2022.128431. https://www.ncbi.nlm.nih.gov/pubmed/35150991.
37. Yang S, Lee S, Lee Y, Cho JH, Kim SH, Ha ES, et al. Cationic nanoplastic causes mitochondrial dysfunction in neural progenitor cells and impairs hippocampal neurogenesis. Free Radic Biol Med. 2023;208:194–210. https://doi.org/10.1016/j.freeradbiomed.2023.08.010. https://www.ncbi.nlm.nih.gov/pubmed/37553025.
38. Le Merre P, Ahrlund-Richter S, Carlen M. The mouse prefrontal cortex: unity in diversity. Neuron. 2021;109 12:1925–44. https://doi.org/10.1016/j.neuron.2021.03.035. https://www.ncbi.nlm.nih.gov/pubmed/33894133.
39. Kamigaki T, Dan Y. Delay activity of specific prefrontal interneuron subtypes modulates memory-guided behavior. Nat Neurosci. 2017;20 6:854–63. https://doi.org/10.1038/nn.4554. https://www.ncbi.nlm.nih.gov/pubmed/28436982.
40. Frankland PW, Bontempi B, Talton LE, Kaczmarek L, Silva AJ. The involvement of the anterior cingulate cortex in remote contextual fear memory. Science. 2004;304 5672:881–3. https://doi.org/10.1126/science.1094804. https://www.ncbi.nlm.nih.gov/pubmed/15131309.
41. Kitamura T, Ogawa SK, Roy DS, Okuyama T, Morrissey MD, Smith LM, et al. Engrams and circuits crucial for systems consolidation of a memory. Science. 2017;356 6333:73–8. https://doi.org/10.1126/science.aam6808. https://www.ncbi.nlm.nih.gov/pubmed/28386011.
42. Miller EK, Cohen JD. An integrative theory of prefrontal cortex function. Annu Rev Neurosci. 2001;24:167–202. https://doi.org/10.1146/annurev.neuro.24.1.167. https://www.ncbi.nlm.nih.gov/pubmed/11283309.
43. Rolls ET. The hippocampus, ventromedial prefrontal cortex, and episodic and semantic memory. Prog Neurobiol. 2022;217:102334. https://doi.org/10.1016/j.pneurobio.2022.102334. https://www.ncbi.nlm.nih.gov/pubmed/35870682.
44. Nihart AJ, Garcia MA, El Hayek E, Liu R, Olewine M, Kingston JD, et al. Bioaccumulation of microplastics in decedent human brains. Nat Med. 2025;31 4:1114–9. https://doi.org/10.1038/s41591-024-03453-1. https://www.ncbi.nlm.nih.gov/pubmed/39901044.
45. Chen YF, Qi RQ, Song JW, Wang SY, Dong ZJ, Chen YH, et al. Sirtuin 7 ameliorates Cuproptosis, myocardial remodeling and heart dysfunction in hypertension through the modulation of YAP/ATP7A signaling. Apoptosis. 2024;29(11–12):2161–82. https://doi.org/10.1007/s10495-024-02021-9. https://www.ncbi.nlm.nih.gov/pubmed/39394530.
46. Zhang Y, Zhou Q, Lu L, Su Y, Shi W, Zhang H, et al. Copper induces cognitive impairment in mice via modulation of Cuproptosis and CREB signaling. Nutrients. 2023;15:4. https://doi.org/10.3390/nu15040972. https://www.ncbi.nlm.nih.gov/pubmed/36839332.
47. Guo B, Yang F, Zhang L, Zhao Q, Wang W, Yin L, et al. Cuproptosis induced by ROS responsive nanoparticles with elesclomol and copper combined with alphaPD-L1 for enhanced Cancer immunotherapy. Adv Mater. 2023;35 22:e2212267. https://doi.org/10.1002/adma.202212267. https://www.ncbi.nlm.nih.gov/pubmed/36916030.
48. Wang W, Lu K, Jiang X, Wei Q, Zhu L, Wang X, et al. Ferroptosis inducers enhanced Cuproptosis induced by copper ionophores in primary liver cancer. J Exp Clin Cancer Res. 2023;42 1:142. https://doi.org/10.1186/s13046-023-02720-2. https://www.ncbi.nlm.nih.gov/pubmed/37277863.
49. Rowland EA, Snowden CK, Cristea IM. Protein lipoylation: an evolutionarily conserved metabolic regulator of health and disease. Curr Opin Chem Biol. 2018;42:76–85. https://doi.org/10.1016/j.cbpa.2017.11.003. https://www.ncbi.nlm.nih.gov/pubmed/29169048.
50. Dreishpoon MB, Bick NR, Petrova B, Warui DM, Cameron A, Booker SJ, et al. FDX1 regulates cellular protein lipoylation through direct binding to LIAS. J Biol Chem. 2023;299 9:105046. https://doi.org/10.1016/j.jbc.2023.105046. https://www.ncbi.nlm.nih.gov/pubmed/37453661.
51. Tian Z, Jiang S, Zhou J, Zhang W. Copper homeostasis and Cuproptosis in mitochondria. Life Sci. 2023;334:122223. https://doi.org/10.1016/j.lfs.2023.122223. https://www.ncbi.nlm.nih.gov/pubmed/38084674.
52. Chen Y, Guo X, Zeng Y, Mo X, Hong S, He H, et al. Oxidative stress induces mitochondrial iron overload and ferroptotic cell death. Sci Rep. 2023;13. https://doi.org/10.1038/s41598-023-42760-4. https://www.ncbi.nlm.nih.gov/pubmed/37726294. 1:15515.
53. Xiong Y, Xiao C, Li Z, Yang X. Engineering nanomedicine for glutathione depletion-augmented cancer therapy. Chem Soc Rev. 2021;50 10:6013–41. https://doi.org/10.1039/d0cs00718h. https://www.ncbi.nlm.nih.gov/pubmed/34027953.
54. Xue Q, Kang R, Klionsky DJ, Tang D, Liu J, Chen X. Copper metabolism in cell death and autophagy. Autophagy. 2023;19 8:2175–95. https://doi.org/10.1080/15548627.2023.2200554. https://www.ncbi.nlm.nih.gov/pubmed/37055935.
55. Xu Y, Liu SY, Zeng L, Ma H, Zhang Y, Yang H, et al. An Enzyme-Engineered nonporous Copper(I) coordination polymer nanoplatform for Cuproptosis-Based synergistic Cancer therapy. Adv Mater. 2022;34 43:e2204733. https://doi.org/10.1002/adma.202204733. https://www.ncbi.nlm.nih.gov/pubmed/36054475.
56. Wang S, Fei H, Ma Y, Zhu D, Zhang H, Li X, et al. Cu-doped polypyrrole hydrogel with tumor catalyst activity for NIR-II thermo-radiotherapy. Front Bioeng Biotechnol. 2023;11:1225937. https://doi.org/10.3389/fbioe.2023.1225937. https://www.ncbi.nlm.nih.gov/pubmed/37485315.
57. Zhang N, Ping W, Rao K, Zhang Z, Huang R, Zhu D, et al. Biomimetic copper-doped polypyrrole nanoparticles induce glutamine metabolism Inhibition to enhance breast cancer Cuproptosis and immunotherapy. J Control Release. 2024;371:204–15. https://doi.org/10.1016/j.jconrel.2024.05.045. https://www.ncbi.nlm.nih.gov/pubmed/38810704.
58. Wong PC, Waggoner D, Subramaniam JR, Tessarollo L, Bartnikas TB, Culotta VC, et al. Copper chaperone for superoxide dismutase is essential to activate mammalian Cu/Zn superoxide dismutase. Proc Natl Acad Sci U S A. 2000;97 6:2886–91. https://doi.org/10.1073/pnas.040461197. https://www.ncbi.nlm.nih.gov/pubmed/10694572.
59. Mlejnek P. Direct interaction between N-Acetylcysteine and cytotoxic Electrophile-An overlooked in vitro mechanism of protection. Antioxid (Basel). 2022;11(8). https://doi.org/10.3390/antiox11081485. https://www.ncbi.nlm.nih.gov/pubmed/36009205.
60. Graham RE, Elliott RJR, Munro AF, Carragher NO. A cautionary note on the use of N-acetylcysteine as a reactive oxygen species antagonist to assess copper

mediated cell death. PLoS ONE. 2023;18 12:e0294297. https://doi.org/10.1371/journal.pone.0294297. https://www.ncbi.nlm.nih.gov/pubmed/38079440.
61. Subramaniam S, Unsicker K. ERK and cell death: ERK1/2 in neuronal death. FEBS J. 2010;277(1):22–9. https://doi.org/10.1111/j.1742-4658.2009.07367.x. https://www.ncbi.nlm.nih.gov/pubmed/19843173.
62. Liu T, Zhu X, Huang C, Chen J, Shu S, Chen G, et al. ERK Inhibition reduces neuronal death and ameliorates inflammatory responses in forebrain-specific Ppp2calpha knockout mice. FASEB J. 2022;36 9:e22515. https://doi.org/10.1096/fj.202200293R. https://www.ncbi.nlm.nih.gov/pubmed/35997299.
63. Li X, Tang C, Ye H, Fang C. Injectable Hydrogel-Encapsulating Pickering emulsion for overcoming Lenvatinib-Resistant hepatocellular carcinoma via Cuproptosis induction and stemness Inhibition. Polym (Basel). 2024;16:17. https://doi.org/10.3390/polym16172418. https://www.ncbi.nlm.nih.gov/pubmed/39274051.

Publisher's note